Supplemental Figure 1

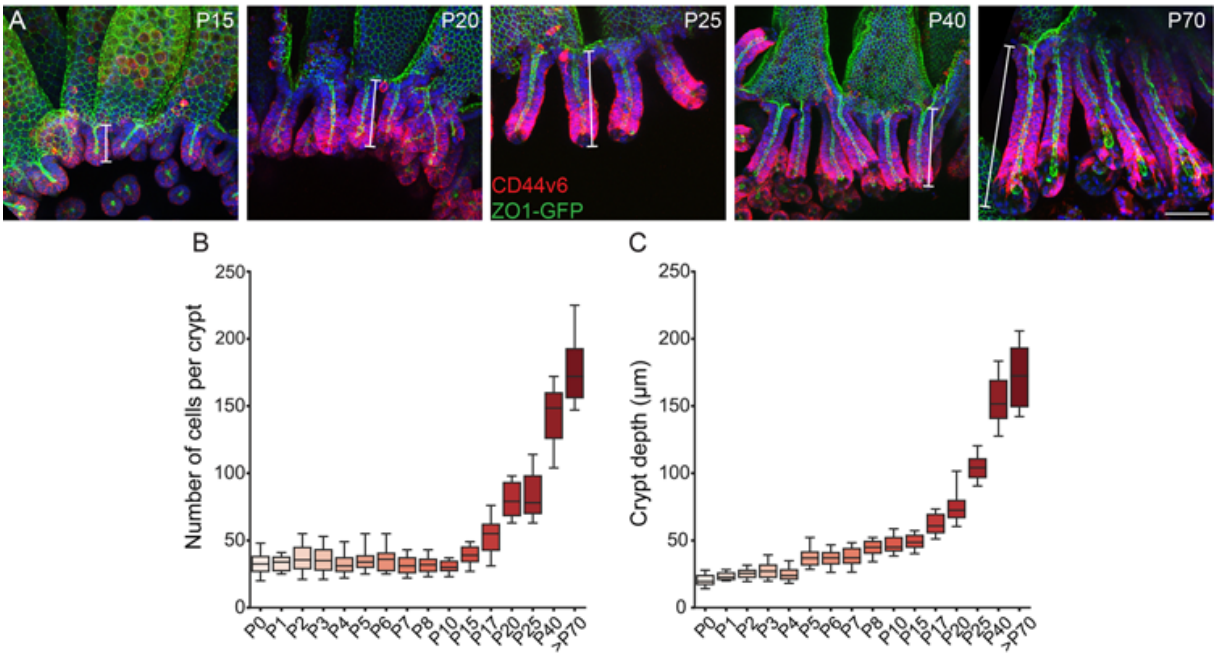

Figure S1, Related to Figure 1. Intestinal crypts undergo expansion after morphogenesis. (A) Epithelial whole mounts of the medial small intestine of ZO1-GFP (green) knockin mice at stages indicated. Epithelial sheets were stained with CD44v6 (red). White brackets highlight the crypt region. (B) Quantification of number of CD44v6+ cells per crypt. (C) Depth of crypts at different stages. All scale bars are 20 µm. For all box and whisker plots, the box boundaries are the 25th and 75th percentiles, and the whiskers are the 5th and 95th percentiles. Total number of mice analyzed were 2-4 mice per stage, with at least 10 crypts per mouse quantified.

Supplemental Figure 2

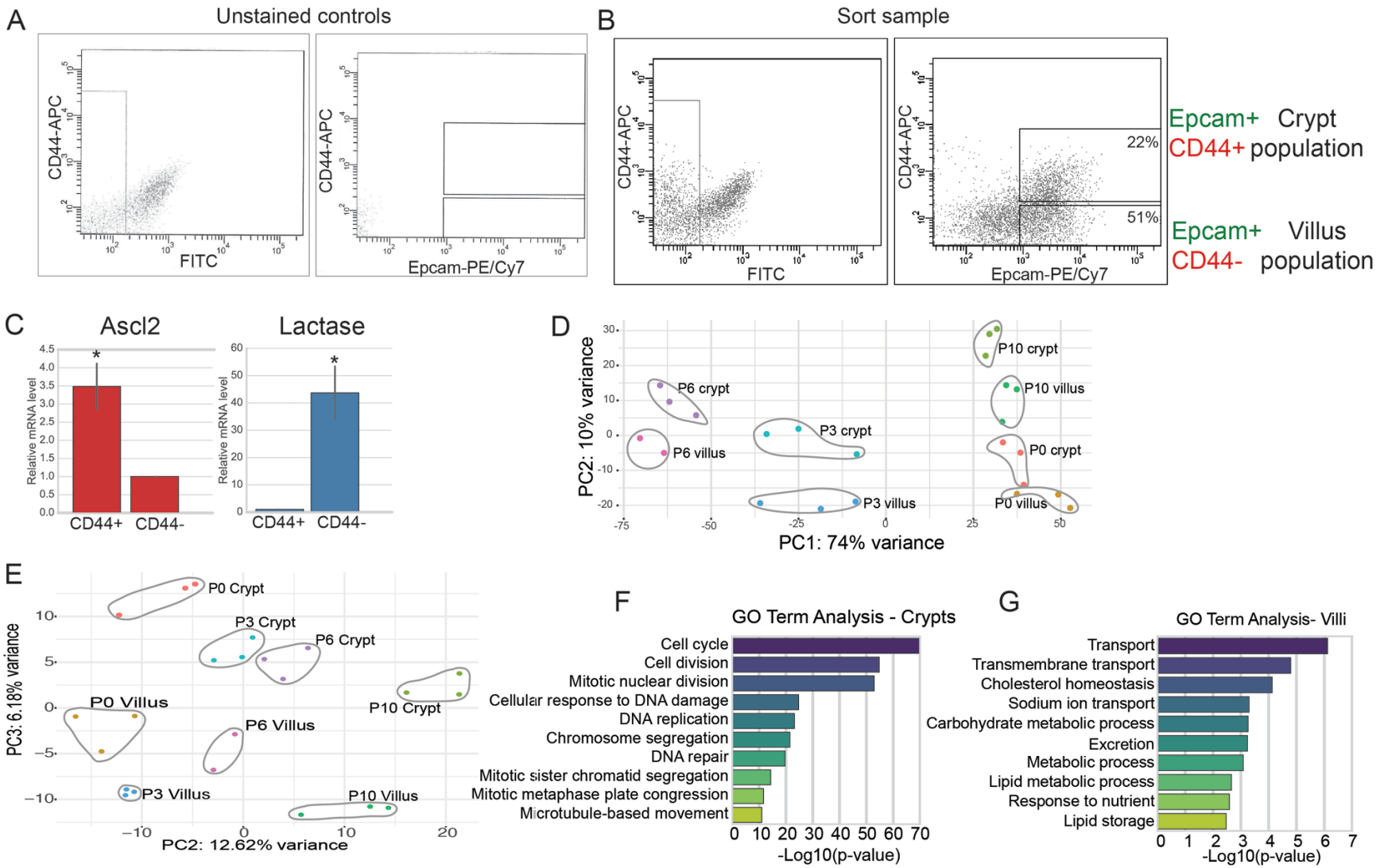

Figure S2, Related to Figure 2. FACs strategy and validation. (A) Representative FACs plot from unstained control intestinal epithelial cells. (B) Representative FACs plot from CD44-APC and Epcam-PE/Cy7-stained intestinal epithelial sheets. Note that FITC was used to detect auto-fluorescence. (C) qPCR analysis of the stem cell marker Ascl2 and the enterocyte marker lactase in sorted cell populations. Error bars are the SEM. *, $p < .05$. (D) Principal component analysis of RNA-seq data of all samples. (E) Scatter plot of Principal component 2 vs. Principal component 3. Note the separation by stage by PC2 and the separation of crypts and villi by PC3. (F) GO term analysis of genes enriched in crypts versus villi at all stages examined. (G) GO term analysis of genes enriched in villi compared to crypts at all stages examined.

Figure S3

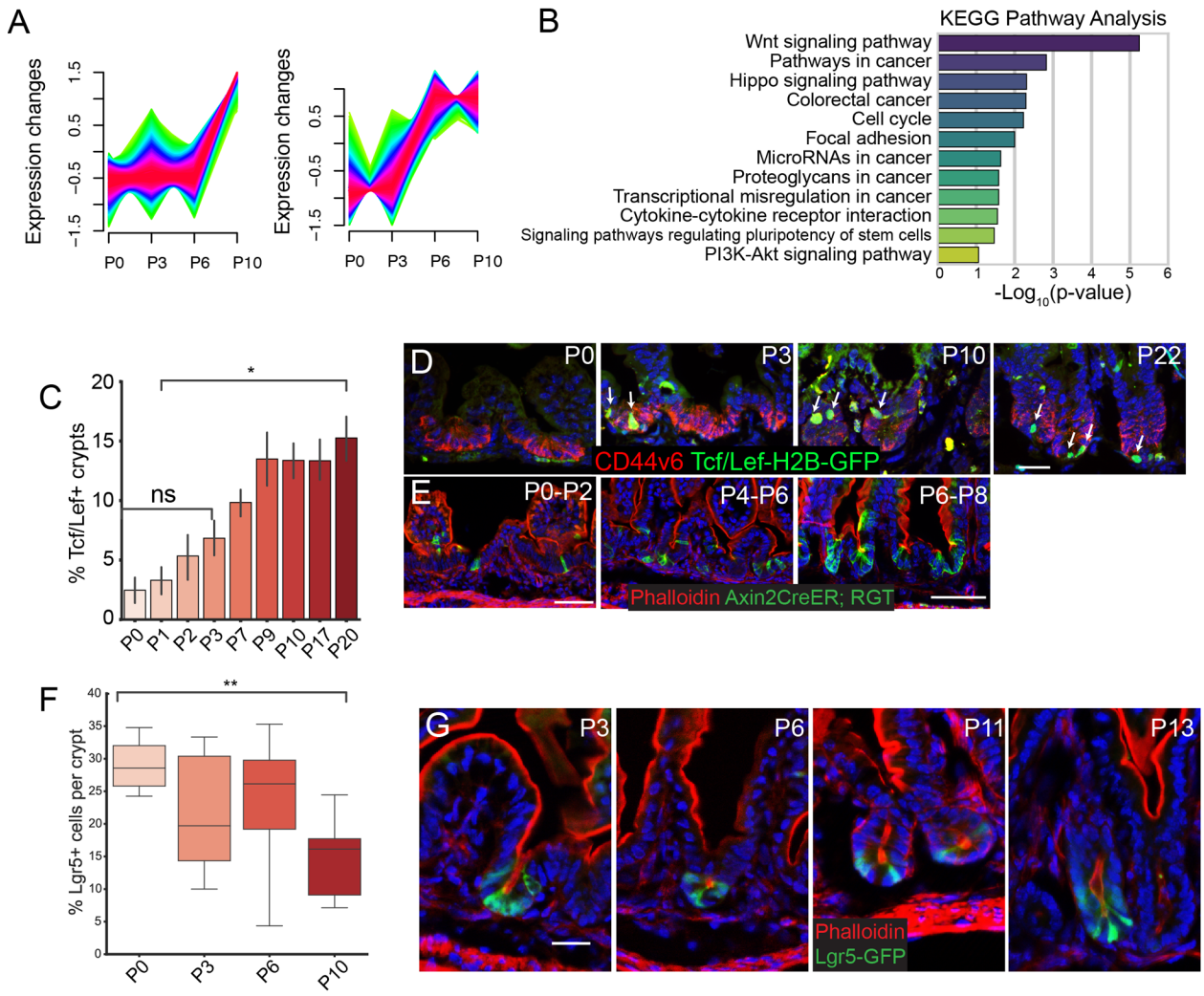

Figure S3, Related to Figure 2. Wnt signaling gene expression is dynamic over crypt morphogenesis. (A) Selected clusters from fuzzy c-means clustering analysis of gene expression in crypts from P0 to P10. (B) KEGG pathway analysis of genes in the clusters shown in (A) that were filtered for genes enriched in crypts compared to villi. (C) Percentage of crypts containing at least one GFP-positive cell, where GFP is driven by a TCF/Lef reporter mouse. A one-way ANOVA test was performed, followed by pairwise Tukey HSD tests. P0 vs. P3 Tukey HSD, ns = not significant. P1 vs. P20 Tukey HSD, *, $p < .05$. (D) Representative images of Tcf/Lef-H2B-GFP signal in postnatal crypts from

P0 to P22. GFP+ cells are marked with arrows. Crypts are labeled with CD44v6 (red). Scale bar, 20 μm. (E) Representative images of GFP signal induced by Axin2CreER. The first stage listed is that at which tamoxifen was injected, the second stage is that when the mice were sacrificed. Phalloidin is in red. Scale bar, 50 μm.(F) Quantification of the percentage of Lgr5-GFP-positive cells per crypt from P0 to P10. A one-way ANOVA test was performed, followed by pairwise Tukey HSD tests. P0 vs. P10 t-test, **, $p < .01$. (G) Representative images of Lgr5-GFP expression in crypts from P3 to P13. Note the bright GFP-positive cells at the base of the crypt at P13. Scale bar, 20 μm.

Figure S4

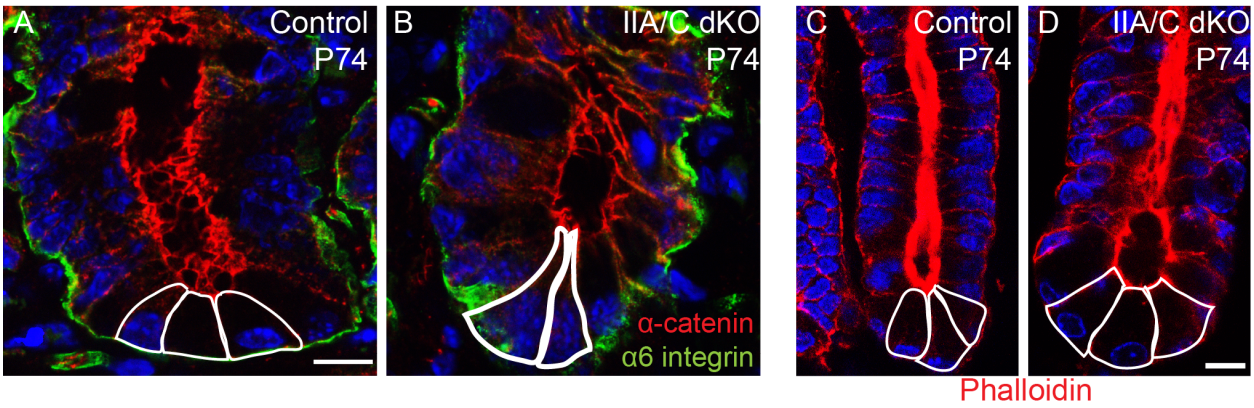

Figure S4, Related to Figure 4. Myosin II is not required to maintain apical constriction of adult crypt cells. (A-B) α6 integrin (green) and α-catenin (red) staining of sections through the base of P74 control (A) and IIA/C dKO (B) crypts after inducing recombination at P69. Cells at the base of the crypt are still apically constricted in the absence of type II myosins. (C-D) Epithelial whole mount images of P74 Control (C) and IIA/C dKO (D) intestines 5 days after tamoxifen injection. Phalloidin is in red. Apically constricted cells are outlined in white. Scale bars, 10 μm.

Figure S5

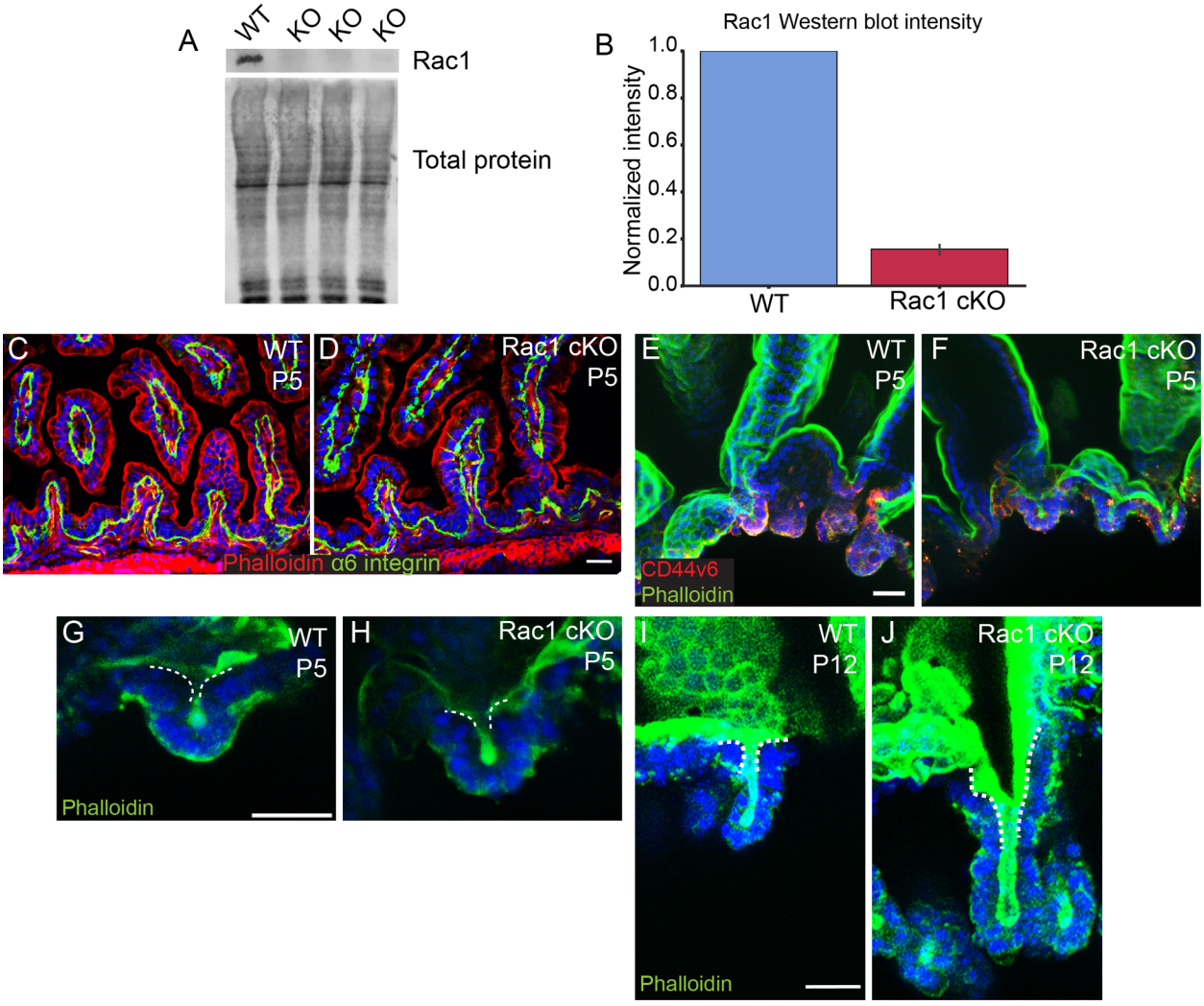

Figure S5, Related to Figure 5. Rac1 cKO intestines are morphologically similar to controls at P5. (A) Western blot of isolated intestinal epithelium from P5 VilCreER; Rac1 fl/fl (Rac1 cKO) or control littermates injected with tamoxifen at P0. The amount of Rac1 (top panel) was normalized to total protein (bottom panel). (B) Graph of quantifications of normalized Rac1 band intensity from control and cKO P5 intestines. (C,D) Sections from WT (C) and Rac1 cKO (D) P5 intestines. Phalloidin is in red and α6 integrin is in green. Scale bar, 20 μm. (E, F) Maximum intensity projections of P5 control (E) or Rac1 cKO (F) intestinal epithelial sheets stained for phalloidin (green) and

CD44v6 (red). Scale bar, 25 μm. Control (G) or Rac1 cKO (H) intestinal sheets at P5 stained for phalloidin (green). The dotted line highlights the initial hinge region. WT intestines have a clearly defined hinge region, which is lost in the P12 Rac1 cKO intestine. Control (I) or Rac1 cKO (J) intestinal sheets at P12 stained for phalloidin (green). WT intestines have a clearly defined hinge region (dotted line), which is lost in the P12 Rac1 cKO intestine.

Figure S6

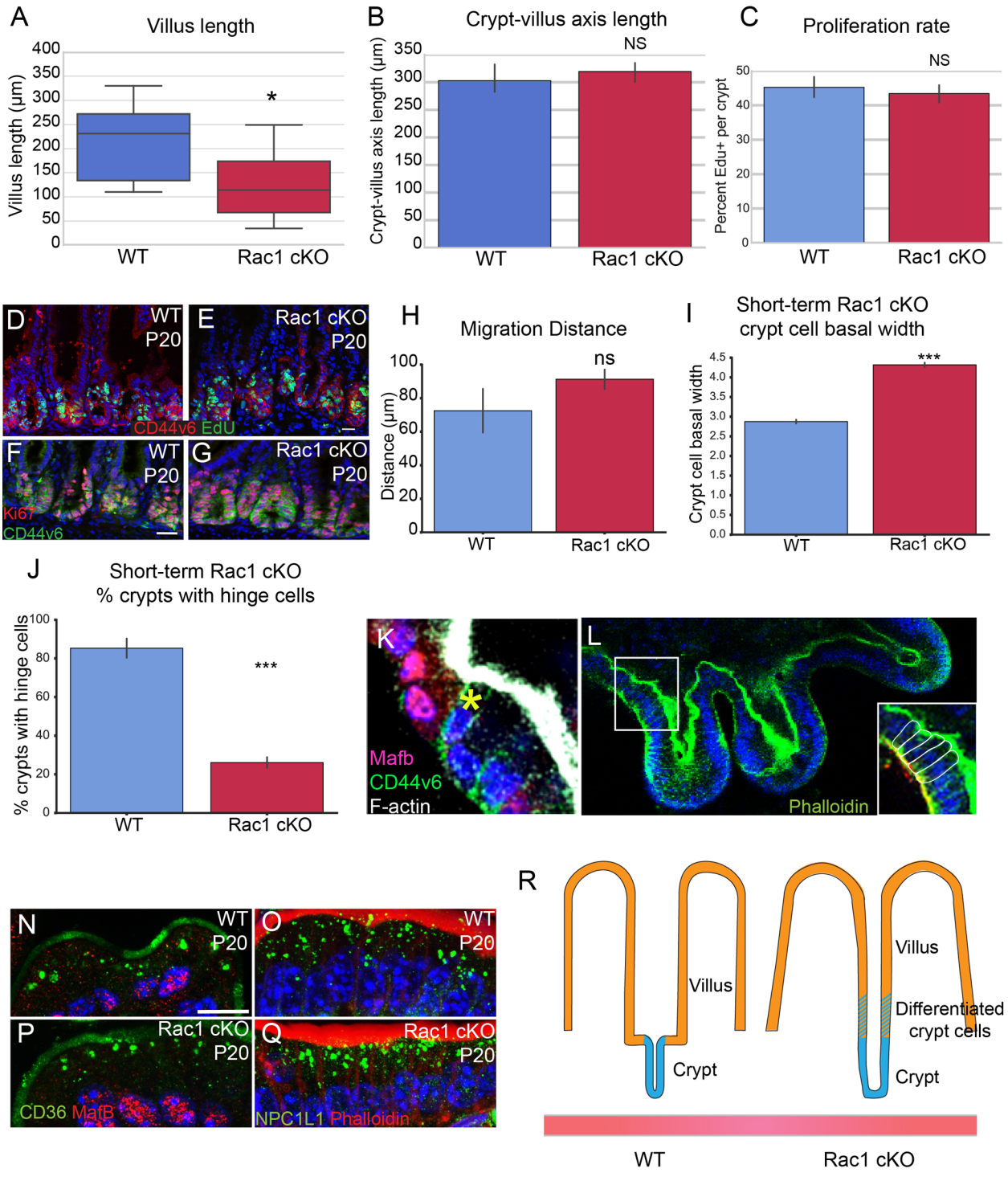

Figure S6, Related to Figure 6. Rac1 cKO intestines do not exhibit proliferation or migration defects. (A) Villus length of WT and Rac1 cKO P20 small intestines. Rac1

cKO villi are statistically significantly shorter than WT villi. T-test, $p < 0.05$. (B) The length of the entire crypt-villus axis is unchanged between WT and Rac1 cKO P20 small intestines. T-test, NS = not significant. (C) Quantification of percent of EdU+ cells per crypt after a 1.5 hour chase. Error bars are the SEM. NS, not significant. (D-E) Representative image of EdU (green) labeling in WT (D) and Rac1 cKO crypts (E)(CD44v6+ region, red) after a 1.5 hour chase. Scale bar is 20 μm. (F-G) Representative images of Ki67 (red) in WT (F) and Rac1 cKO (G) crypts (marked with CD44v6, green). Scale bar is 20 μm. (H) Bar plot of the absolute distance of BrdU+ cells from the crypt base after a 24-hour chase. Distances labeled were averaged across all BrdU+ cells (> 137 cells) per mouse. Plot is an average of three mice per genotype. (I) Quantification of crypt cell basal width in P12 WT and Rac1 cKO mice injected with tamoxifen at P10. (J) Quantification of the percent of crypts with identifiable hinge cells in P12 WT and Rac1 cKO mice injected with tamoxifen at P10. (K) Hinge cell (marked with an asterisk) exists at the boundary between CD44v6-positive cells (green) and MafB-positive cells (red). (L) Rac1 knockout organoid with inset demonstrating a lack of wedge-shaped cells at the “top” of the crypt. (N-O) Staining of the lipid transporter CD36 (green) (N) and the cholesterol transporter NPC1L1 (green) (O) in WT intestines. For (N), MafB is in red, and for (O), Phalloidin is in red. (P) Staining of CD36 (green) in Rac1 cKO P20 intestines. MafB is in red. Scale bar, 10 μm. (Q) Staining of NPC1L1 (green) in Rac1 cKO P20 intestines. Phalloidin is in red. (R) Model of the differences in intestinal architecture in the Rac1 cKO mutant.

Figure S7

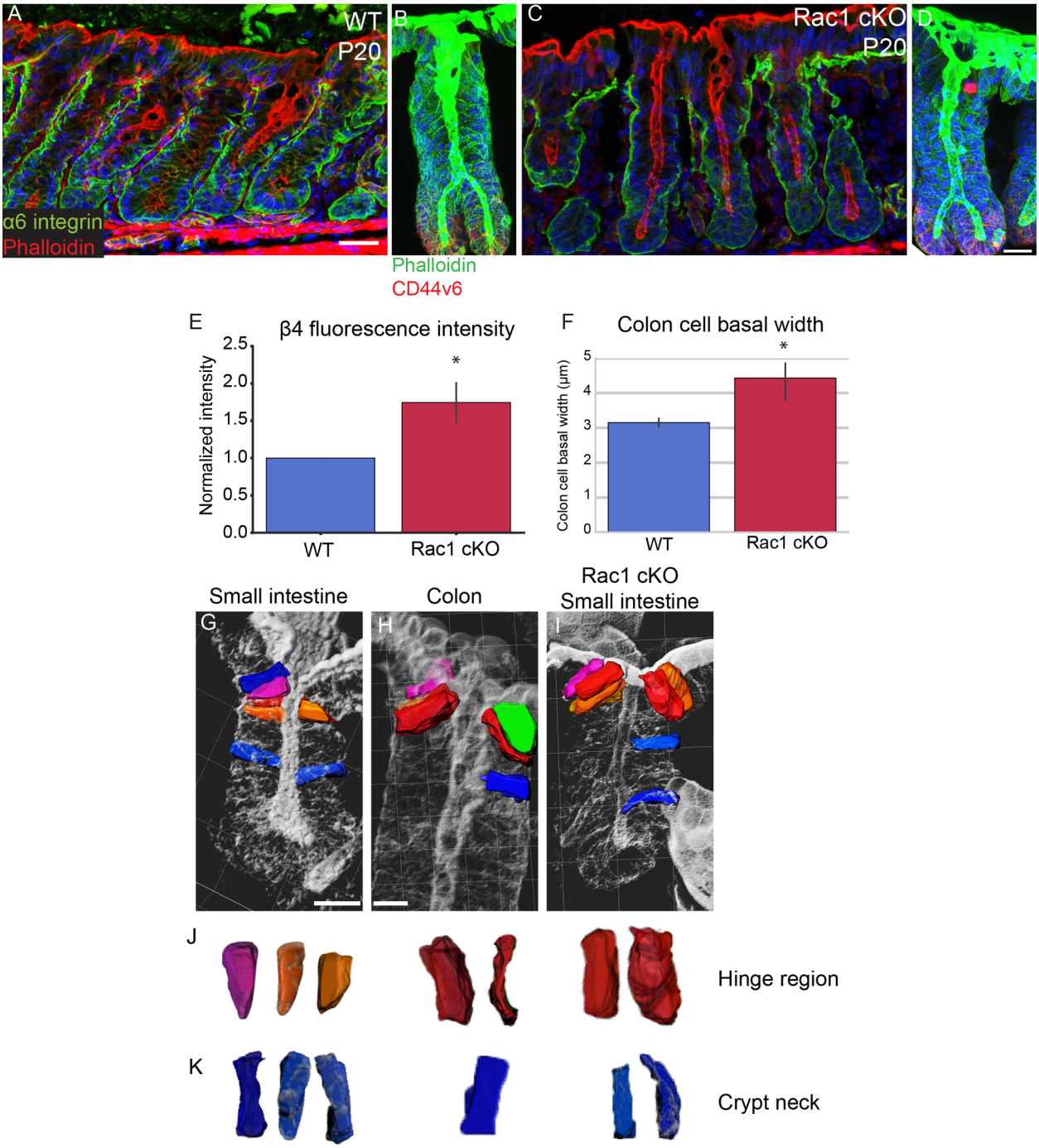

Figure S7, Related to Figure 6. The colon is unaffected by loss of Rac1. Sections from WT (A) and Rac1 cKO (C) P20 colons. Phalloidin is in red and α6 integrin is in green. Scale bar is 50 μm. (B,D) Maximum intensity projections from colon epithelial

whole mounts from WT (B) and Rac1 cKO (D) P20 colons. Phalloidin is in green and CD44v6 is in red. Scale bar is 20 μm. (E) Quantification of the normalized fluorescence intensity of β4 integrin in WT and Rac1 cKO P20 colons. Error bars are the SEM. *, $p < .05$ by student's t-test. (F) Quantification of the basal width of colonocytes in WT and Rac1 cKO P20 colon crypts. *, $p < .05$ by student's t-test. (G) Surface rendering of cells in the neck (blue) and hinge (pink/orange) region of a small intestine crypt. (H) Surface rendering of cells at the mouth of the colon crypt (red). Notably, colonocytes are not basally constricted and apically expanded. A surface rendering of a Goblet cell (green) shows that Goblet cells are apically expanded. (I) Surface rendering of cells in the neck (blue) or hinge region (red/orange) of P20 Rac1 cKO small intestine. Cells in the hinge region are not basally constricted or apically expanded. (J,K) Representative surface renderings of single hinge cells (J) or crypt neck cells (K) in the small intestine, colon, or Rac1 cKO small intestine.

Table S1. Contractility-associated genes enriched in P0 crypts compared to P0 villi. Related to Figure 3.

Gene	*Fold change*
Anln	5.12
Aspm	4.33
Plk1	4.14
Ect2	4.09
Tpm2	4.08
Kif23	3.96
Aurkb	3.52
Racgap1	3.41
Diaph3	3.31
Myl9	3.28
Cit	3.04
Ptk7	3.02
Pardg6	3.00
Flna	2.99
Cnn3	2.23
Diaph2	2.22
Pls3	2.14
Cnn1	2.08
Prkci	2.04
Arhgef17	1.99
Pak6	1.96
Pdlim1	1.90
Dmpk	1.86
Arhgap35	1.78
Pdk1	1.72
Llgl1	1.67
Myh9	1.63
Ppp1cb	1.59
Arhgap5	1.58
Sept2	1.54
Ywhag	1.53
Pak2	1.52
Calm2	1.51
Emd	1.51

Table S2. Contractility-associated genes enriched in P0 crypts compared to P3 crypts. Related to Figure 3.

Gene	*Fold change*
Myh14	8.11
Tpm2	6.73
Myl9	4.13
Cnn1	3.85
Myh9	3.78
Arhgef17	3.68
Ptk7	3.16
Llgl1	3.14
Plk1	2.51
Flna	2.38
Cit	2.37
Pak6	2.00
Dmpk	1.63
Ywhag	1.55